Colloid and Interface Science Communications 47 (2022) 100594

Contents lists available at ScienceDirect

Colloid and Interface Science Communications

journal homepage: www.elsevier.com/locate/colcom

Rapid Communication

A versatile strategy for loading silica particles with dyes and quantum dots

Hui Yang [a,b], Eser Metin Akinoglu [c,a,*], Fabio Lisi [c,d], Lihua Wu [a], Shitao Shen [b], Mingliang Jin [a,b], Guofu Zhou [b], Michael Giersig [a,e], Lingling Shui [f], Paul Mulvaney [c]

[a] International Academy of Optoelectronics at Zhaoqing, South China Normal University, Zhaoqing, 526238, Guangdong, PR China
[b] Guangdong Provincial Key Laboratory of Optical Information Materials and Technology & Institute of Electronic Paper Displays, South China Academy of Advanced Optoelectronics, South China Normal University, Guangzhou 510006, PR China
[c] ARC Centre of Excellence in Exciton Science, School of Chemistry, University of Melbourne, Parkville, VIC 3010, Australia
[d] Institute of Industrial Science, The University of Tokyo, 153-8505 Tokyo, Japan
[e] Institute of Fundamental Technological Research, Polish Academy of Sciences, 02-106 Warsaw, Poland
[f] Guangdong Provincial Key Laboratory of Nanophotonic Functional Materials and Devices, School of Information and Optoelectronic Science and Engineering, South China Normal University, Guangzhou 510006, Guangdong, PR China

ARTICLE INFO

Keywords:
Silica particles
Dye
Quantum dot
Polydiallyldimethylammonium chloride
Doping
Loading

ABSTRACT

A simple and inexpensive method for the controlled loading of silica particles with dyes and nanocrystals is presented. Polydiallyldimethylammonium chloride is used as a positively charged bridge to facilitate electrostatic adsorption of negatively charged dyes onto negatively charged silica microspheres. The particles are subsequently coated with a further silica shell to protect the dyes against chemical degradation and leakage and this shell affords a unform particle surface independent of its doping. This encapsulation method is highly versatile and can be extended to doping with semiconductor nanocrystals, which we demonstrate using CdSe/ZnS core/shell quantum dots. The synthesis steps and end products are characterized with electron microscopy, optical spectroscopy and the electrokinetic potential of the colloidal suspensions. We show that the particles adapt the optical properties of their dopants and are resistant to degradation, dopant leakage and show reasonable emission even at acidic pH values due to the protective shell.

1. Introduction

Chromatic and photoluminescent silica particles are important in a wide range of applications such as biomedicine [1–5], sensor technologies [2,6] and electronic applications [4]. A key reason for their popularity is their photostability, water solubility, low toxicity, and ease of chemical functionalization [5]. To this end, a variety of strategies have been developed to incorporate dye molecules and photoluminescent materials such as quantum dots (QDs) into silica nanoparticles including covalent coupling [8,9,10], electrostatic attraction [7,11,12] and reverse microemulsion synthesis [13,14].

Covalent coupling involves the incorporation of amino-reactive dyes into silica particles, using a silane agent, such as 3-aminopropyltriethoxysilane (APS) to form a dye-APS precursor, and then APS and tetraethoxysilane (TEOS) are simultaneously hydrolyzed and condensed to form silica particles [8,9]. However, during this synthesis route, the hydrolysis and condensation rate of APS is much lower than that of TEOS, and when TEOS is completely condensed, most of the dye-APS precursors remain in the solution limiting the dye doping efficiency to only ~6–13% [10]. Further limitations are the long reaction times (> 12 h) and relatively costly amine reactive dyes [11].

An alternative approach exploits the negative surface charge on silica particles prepared by the Stöber method [12]. It is relatively simple to adsorb positively charged dyes onto these silica particle surfaces, however the method is inherently limited due to the fact that many water-soluble dyes are negatively charged and cannot be directly coated onto the silica particles [13]. Nevertheless, positively charged dyes such as Ru(II) complexes have been successfully incorporated into silica nanoparticles by electrostatic interaction in a one-pot synthesis by adding the Ru(II) complexes into the solution during the Stöber synthesis [7,14]. Ru(II) dyes are notoriously expensive while numerous less-expensive dyes such as Rhodamine B, which acquire a positive charge at neutral pH, are only very weakly charged in the required alkaline medium, rendering them unsuitable for electrostatic adsorption during the Stöber process [15,16].

An alternative approach is to carry out the synthesis in inverse

* Corresponding author at: ARC Centre of Excellence in Exciton Science, School of Chemistry, University of Melbourne, Parkville, VIC 3010, Australia.
E-mail address: e.a@fu-berlin.de (E.M. Akinoglu).

https://doi.org/10.1016/j.colcom.2022.100594
Received 9 November 2021; Received in revised form 29 December 2021; Accepted 24 January 2022
Available online 11 February 2022

microemulsions. This method is based on the use of surfactant-stabilized water droplets dispersed in an oil phase to form nanoreactor micelles. Silica particle nucleation and growth occur within the aqueous droplets [9]. The aqueous phase nanoreactors contain both the ammonia catalyst and the dissolved dyes. Dye incorporation occurs as TEOS diffuses into these nanoreactors and hydrolyzes and condenses to form silica particles. Drawbacks of this method include the additional cost and environmental footprint of the excessive organic solvent and surfactant use, dye leakage from the silica matrix, the difficulty of purifying the colloid of residual surfactants and oil, and the limited range of particle sizes (20–200 nm), which is governed by the size of the nanoreactors [22,23].

The incorporation of photoluminescent QDs into silica particles has also been achieved through a variety of methods. Silica coated QDs (i.e. core-shell nanoparticles) represent the simplest material system but their synthesis is limited to relatively small nanoparticle sizes, and the limitation of only one QD per particle is an obstacle for applications requiring large particle sizes with strong photoluminescence [17]. A larger number of QDs was successfully loaded into the bulk of silica nanoparticles by Wang et al. [18] via the reverse microemulsion synthesis method. Doping of QD and other nanoparticles into large silica particles was also achieved by adsorbing nanoparticles onto a preformed silica particles with subsequent silica shelling. For example, Kim et al. [19], Ha et al. [20] and Jun et al. [21] used thiol functionalized silica particles to bind QDs onto the silica particle surface, and Yoo et al. [22] showed that ligand-exchanged QDs with mercaptopropionic acid were self-assembled on an aminopropyl-functionalized silica sphere using electrostatic interactions, which were then centrifuged and redispersed in ethanol, and a subsequent sol–gel reaction using tetraethoxysilane produced a silica shell. Finally, they used a sol–gel reaction utilizing trimethoxy(2-phenylethyl)silane for phenylethyl-functionalization of the particles. On the other hand, Rühl and coworkers [23] demonstrated the controlled embedding of multiple nanoparticles in silica colloids using hydrophobic or hydrophilic stabilized nanoparticles adsorbed with amphiphilic poly(vinylpyrrolidone) (PVP), which were subsequently adsorbed on silica spheres and covered by variable-thickness silica shells.

In this work, we propose a versatile method to incorporate affordable, negatively charged dyes into silica particles to obtain chromatic silica particles. We take advantage of the negative charge of both the silica particles and the dyes, and electrostatically couple them with the strongly positively charged polymer polydiallyldimethylammonium chloride (PDADMAC), which acts as a bridge. We adsorb pigments, dyes and nanocrystals around the surface of monodisperse and uniform seed silica particles instead of incorporating them into the bulk of the particles. This effectively circumvents the adverse effects of the dye on the nucleation and growth of the silica particles, allowing a better control of the size distribution. Finally, the loaded silica particles are terminated with a silica shell forming a core-shell-shell particle. The outermost silica layer of the particles ensures effective encapsulation of the dyes, and most importantly provides a benign termination that can be post-functionalized as required. Furthermore, we demonstrate the flexibility of this strategy by expanding it to QD-doped silica particles. The uniform surface termination, monodispersity and straightforward loading of the dye or quantum dot into silica particles prepared by this inexpensive method render them ideal for biological imaging and monitoring, and electronic applications such as reflective displays operating on electrokinetic principles.

2. Experimental section

2.1. Materials

Tetraethyl orthosilicate (TEOS, 99.999%), ammonium hydroxide solution (30%), absolute ethanol (Abs. EtOH, 99.9%), Direct Blue 71 (Dye content $\geq$ 50%), amaranth (Dye content 85–95%), tartrazine (Dye content $\geq$ 85%), poly(diallyldimethylammonium chloride) solution (PDADMAC, average Mw <100,000, 35 wt% in H_2O), sodium chloride (NaCl, $\geq$99.5%), cadmium oxide (99.99%), selenium (99.5%,100mesh), trioctylphosphine oxide (TOPO, 90%), tributylphosphine (TBP, 97%), 1-octadecene (ODE), octadecylamine (ODA, 97%), stearic acid (99%), poly(styrene-*co*-maleic anhydride) terminated with cumene (PSMA, ~1700 g/mol), analytical grade(AR) chloroform ($CHCl_3$), ethanolamine (EA, 97%) were all purchased from Sigma-Aldrich and used without any further purification. 18 MΩ ultrapure Milli-Q water was used for all experiments.

2.2. SiO_2 NP synthesis

Hydrophilic SiO_2 particles were prepared based on our earlier work which utilizes Dean flow mediated ultra-fast mixing in a spiral microchannel [24]. In short, a solution A consisting of 10 mL ammonia water in 20 mL pure ethanol and a solution B consisting of 2 mL TEOS in 32 mL pure ethanol was prepared. These two reactant solutions were introduced into syringes for insertion into the microfluidic spiral reactor at a speed of 400 μL/min. The micromixer was placed into a thermostatted water bath at a constant temperature $T = 40$ °C. The exiting, mixed solution was kept flowing inside an extended polytetrafluoroethylene (PTFE) tube to prolong the residence time and enable SiO_2 particle growth. The different sizes of the SiO_2 particles were controlled via the concentration of TEOS and the temperature during the synthesis.

2.3. QD synthesis

Colloidally stable, water-soluble, biocompatible, semiconductor nanocrystals were prepared according to a previously reported method [25,26]. First, CdSe/ZnS core/shell QDs with three ZnS shells were synthesized [32,33]. Subsequently, these QDs were transferred into water utilizing a low molecular weight, amphiphilic polymer coating (PSMA) to render them water soluble while at the same time preserving their optical spectra, photoluminescence intensities and colloidal stability over a wide pH range (pH 3–13) [25]. To this end, CdSe/ZnS QDs in $CHCl_3$ (50 nmol) were added to 5 μmol PSMA pre-dissolved in $CHCl_3$ to ensure a 100-fold molar excess of PSMA. The reaction mixture (~1 mL) was tumbled at room temperature for at least 3 h. A 2 mL portion of water containing 20 μL ethanolamine was added to the above solution and tumbled for 30 min at room temperature, after which the QDs had transferred into the water phase owing to hydrolysis of the PSMA which creates a negatively-charged polymeric shell. The sample was centrifuged to speed up the separation of $CHCl_3$ and water phases. The aqueous phase was then collected and the excess polymer was removed using a centrifugal filter (Amicon, 30 kDa MWCO). Finally, the aqueous QD solution was passed through a 0.22 μm filter to remove any aggregates.

2.4. Fabrication of SiO_2@Dyes

Route (*i*): Direct Blue 71, amaranth or tartrazine aqueous solutions (0.5 mL, 3×10^{-3} M) were mixed with 1 mL ethanol and 100 μL of PDADMAC aqueous solution (30 mg/mL) and stirred for 0.5 h to allow binding of the dyes onto the PDADMAC chains. Then, 0.5 mL of dye/PDADMAC solution were rapidly added into a 10 mL SiO_2 particles aqueous solution (10 mg/mL) in a glass flask for 1 min. Subsequently, the mixture was stirred at room temperature for 30 min to enable electrostatic adsorption of the dye/PDADMAC onto the SiO_2 particles. Afterwards, the product solution was repeatedly washed with ultrapure water and centrifuged at 5600 *g* to remove any excess dye and PDADMAC, and then finally redispersed into ethanol.

Route (*ii*): 1 mL PDADMAC aqueous solution (30 mg/mL) and 10 mL SiO_2 particles (10 mg/mL) were mixed for 30 min to obtain SiO_2@PDADMAC particles. Then dyes in aqueous solution (3×10^{-3} M) were added to the SiO_2@PDADMAC particle solution, with subsequent magnetic stirring for 30 min to form SiO_2@PDADMAC@dye particles.

Finally, a wash step with ethanol was performed to remove excess unbound dye, followed by redispersion into pure ethanol.

2.5. Preparation of quantum dot doped silica

The coating of SiO_2 particles with a variety of nanoparticles was facilitated by use of a cationic polyelectrolyte as a binder. Firstly, 1 mL PDADMAC aqueous solution (30 mg/mL) and 10 mL SiO_2 particles (10 mg/mL) were mixed for 30 min to obtain SiO_2@PDADMAC particles. Then 0.5 mL CdSe/ZnS 250 nM aqueous solution was added to the SiO_2@PDADMAC particle solution, with subsequent magnetic stirring for 30 min to form SiO_2@PDADMAC@QDs particles. Finally, a wash step with ethanol was performed to remove any un-adsorbed nanocrystals, followed by redispersion into pure ethanol.

2.6. Silica shelling of SiO_2@Dyes and SiO_2@PDADMAC@QDs

Firstly, the nanoparticles were mixed into a solution of 10 mL ethanol, 815 μL ultrapure water, 80 μL TEOS and 100 μL $NH_3{\cdot}H_2O$. The mixture was stirred at 30 °C for 12 h. Then the SiO_2 particles were centrifuged for 5 min at 5600 *g* and redispersed into ultrapure water for several times to remove any unreacted precursors.

2.7. Characterization

All characterization measurements were carried out at room temperature. The zeta-potentials (ζ) of the samples were measured in ultrapure H_2O (pH = 6.8) containing 10^{-2} M NaCl with a Brookhaven ZetaPALS apparatus. A ZEISS Sigma 500 scanning electron microscope (SEM) was used to determine the particle uniformity and size, and the samples were prepared by drop casting the aqueous particle dispersion onto a 5 mm × 5 mm sized silicon wafer and left to dry in air at room temperature. Transmission electron microscopy (TEM) images were recorded with a JEOL-2010 electron microscope operating at 200 kV. The absorption and reflection spectra of the films were measured using a UV/VIS/NIR spectrophotometer (Perkin Elmer Lambda 1050) equipped with an integrating sphere. The absorbance measurements of QD loaded silica particle suspensions were conducted in a mixed solution of toluene and ethanol in a 1:1 volume ratio for refractive index matching, which reduces the light scattering contribution in the extinction spectra. The remaining light scattering background was subtracted using a background fit assuming Rayleigh scattering.

3. Results and discussion

Different size silica particles were prepared via a previously reported protocol using a spiral microreactor (Fig. 1a) [24]. These silica particles are negatively charged because of ionization of the surface hydroxyl groups. Commercial water-soluble anionic dyes, i.e. Direct Blue 71, amaranth and tartrazine, were used to coat the silica particles through electrostatic adsorption. We employed PDADMAC as a binding agent, which was utilized in two different ways. In the first case, PDADMAC was premixed with the respective dye, as schematically shown in Fig. 1b. Because of their opposite electrostatic charge, the PDADMAC and dyes electrostatically adsorb and form a soluble PDADMAC/dye composite in aqueous solution. An excess of PDADMAC ensured that these composites

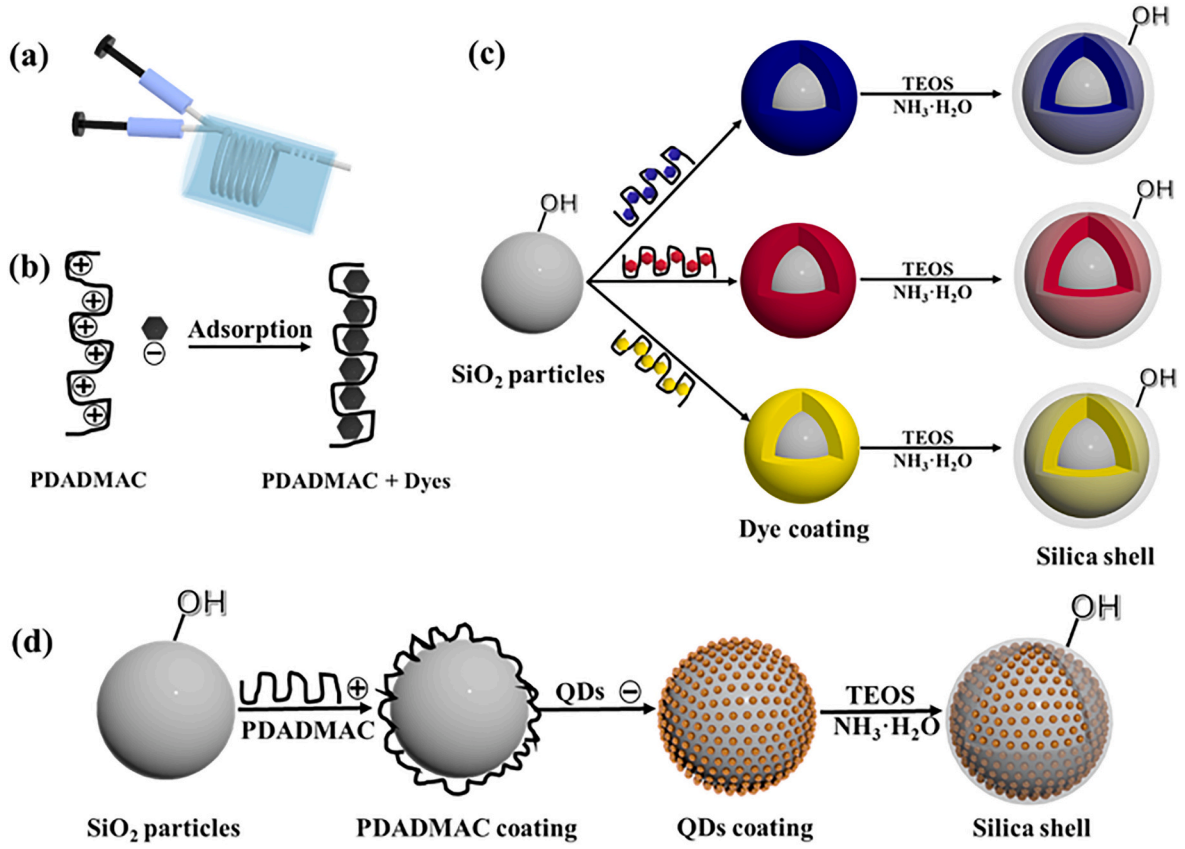

Fig. 1. Schematic illustration of the process used for coating silica nanoparticles with dyes or quantum dots. (a) the spiral microreactor used for the core SiO_2 nanoparticle synthesis. (b, c): Illustration of Route (i) PDADMAC and dyes are first electrostatically bound to form a composite. Then the PDADMAC/dye composite is adsorbed onto the silica particles followed by the growth of a silica shell to terminate the particle surface. Use of magenta, cyan and yellow dyes enables full spectrum silica particles to be synthesized. (d) Route (ii): PDADMAC is adsorbed on the silica particles to reverse the charge on the core particles, followed by the adsorption of quantum dots. The surface is then terminated with a silica shell. (For interpretation of the references to colour in this figure legend, the reader is referred to the web version of this article.)

remained positively charged and could electrostatically adsorb as a composite onto the silica particles (Fig. 1c). In the second case, PADMAC was allowed to adsorb to the silica seed particles first, reversing the zeta potential of the particles. The respective anionic dyes were then allowed to electrostatically adsorb onto the silica particles to form a "pigment shell" (**Fig. S1**). In both cases, a second silica shell was formed via Stöber growth to protect the dyes and to provide a homogeneous surface chemistry for the particles. The quantum dot loading followed route (ii) and is shown in Fig. 1d. The process was monitored with zeta potential measurements shown in Fig. 2. The change in zeta potential is an indicator for the success of the electrostatic adsorption step. For the route employing the PDADMAC/dye composite, the change in zeta potential is shown in the bar chart in Fig. 2a, where C, M, and Y stand for the cyan dye Direct Blue 71, the magenta dye amaranth and yellow dye tartrazine respectively, while the symbol S represents the pristine silica particles, and S@P/D represents silica particles encapsulated with a PDADMAC/dye composite shell, while S@P/D@S denotes the silica terminated products. The initial silica particles are negatively charged with $\zeta \approx -58$ mV. After electrostatic adsorption of the PDADMAC/dye composites, $\zeta > +50$ mV for all S@P/D indicating successful adsorption. Formation of an outer silica shell gives $\zeta < -50$ mV, so that the sequential preparation of silica@dye particles via route (*i*) yields highly charged, colored particles as shown in Fig. 2b. The consistently large negative or positive value of ζ during each synthesis step is crucial for ensuring long-term colloidal stability of the suspension. Zeta potentials collected on particles undergoing route (ii) are presented in the bar chart in **Fig. S2 a**. Here, S@P represents PDADMAC coated silica particles, S@P@D represents dye coated S@P particles, and S@P@D@S represents the silica terminated product. As before, the initial silica particles are uniformly anionic with $\zeta \approx -58$ mV. After electrostatic adsorption of the PDADMAC, $\zeta > +50$ mV, which is slightly reduced to $\zeta > +30$ mV after anionic dye adsorption. Formation of an outer silica shell gives $\zeta < -50$ mV, so that the sequential preparation of dye loaded silica particles via route (*ii*) also yields highly charged, colored particles as shown in **Fig. S2b**. However, a distinct difference can be seen in the visible appearance of the dye loaded silica particle solutions prepared by the two different routes as shown in Fig. 2b and **Fig. S2 b**. Clearly, route (*i*) results in a more intensely colored suspension which suggests higher dye adsorption via route (*i*) as compared to route (*ii*). We attribute this to the fact that route (*ii*) only enabled the adsorption of a dye monolayer whereas route (*i*) enabled adsorption of aggregated PDADMAC/dye composites, which ultimately led to a higher concentration of dyes on the silica particles. We further investigated the maximum electrostatic adsorption of the PDADMAC/dye composite on the silica particles via route (*i*). To this end, we sequentially added the respective PDADMAC/dye composite solutions to a silica particle solution and monitored the zeta potential after 20 min adsorption time, which is shown in Fig. 2c. The silica particles initially exhibited a zeta potential $\zeta \approx -55$ mV, which decreased in magnitude monotonically with the addition of the cationic PDADMAC/dye composites. The formation of a plateau at about $\zeta \approx -50$ mV indicates the maximum absorption of the respective PDADMAC/dye composites, and also implies that the adsorption of the particles shown in Fig. 2a corresponds to surface saturation. From Fig. 2c, it is evident that Direct Blue 71 and amaranth follow a similar trend, whereas tartrazine saturation requires more than twice the dye concentration. Because the binding of the dyes to the PDADMAC is governed by their electrostatic interaction, we can conclude that this interaction is smaller between tartrazine and PDADMAC, as compared to PDADMAC and Direct Blue 71 or amaranth. This can be explained by the molecular structure of the dyes shown in **Fig. S3**. They are in a salt form and the highlighted -COONa groups on the tartrazine completely ionize into $-COO^-$ and Na^+ in an aqueous solution, but the ionized $-COO^-$

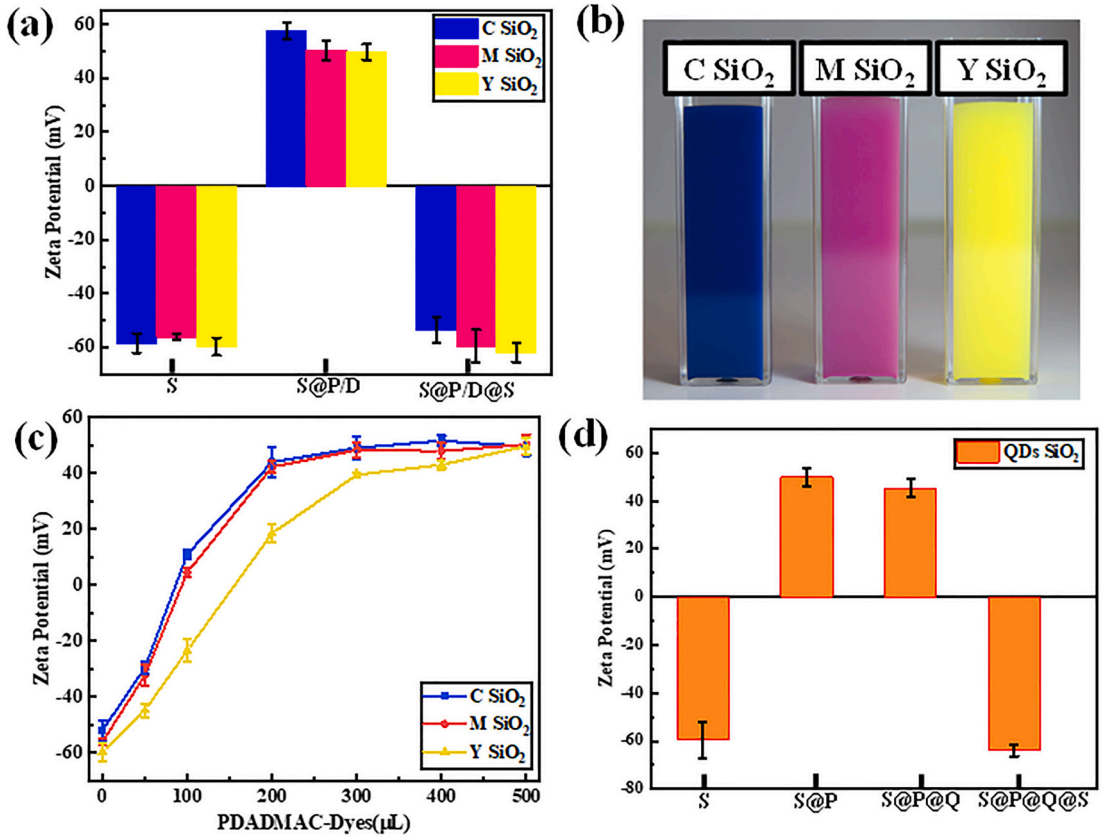

Fig. 2. Sequential shell formation around silica particles monitored by zeta-potential measurements. (a) Dye binding via route (*i*). Anionic silica particles are first shelled in a cationic PDADMAC/dye composite and then in an anionic silica shell. (b) Photograph of dye loaded particles prepared via route (*i*). (c) Zeta-potential vs. dye loading via route (*i*). (d) Quantum dot loading via route (*ii*).

undergoes a hydrolysis process to generate -COOH. However, the -SO_3Na groups on all dyes completely ionize into -SO_3^- and Na^+ in an aqueous solution, and the -SO_3^- remains charged as it does not easily hydrolyze. Because the charging effect of -SO_3Na is stronger than that of -COONa, it is expected that Direct Blue 71 with four -SO_3Na functional groups, and amaranth with three -SO_3Na functional groups, are more effectively loaded than tartrazine with two -SO_3Na and one -COONa functional group. This is indeed reflected in Fig. 2c, where the loading saturation level of tartrazine is 2.5-fold that of Direct Blue 71 and amaranth. We calculated the loading amount of the dyes based on the initial concentration of the dye and the adsorption saturation concentration. The dye concentration of the PDADMAC-Dyes mixed solution is 0.94 mM in all cases, the Direct Blue 71 and amaranth dyes reached the adsorption saturation value near 1.88 nmol/mg (dye concentration per silica particle concentration), and tartrazine reached the adsorption saturation value near 4.7 nmol/mg. Aside from the binding of these dyes on the silica particles, we also explored the binding of CdSe/ZnS quantum dots onto the silica particles. We found that route (*i*) is not suitable due to QD aggregation which occurs as soon as the QDs are mixed with PDADMAC solution; however route (*ii*) offers a viable protocol for loading the silica particles with nanocrystals. As before, we monitored the zeta potential for each sequential adsorption step, and this is summarized in the bar chart in Fig. 2d. The trend in ζ is equivalent to route (*ii*) for the dyes (**Fig. S1**) and indicates successful quantum dot loading to the silica particles with subsequent silica shell encapsulation.

To investigate the QD loading efficiency, different amounts of QDs were loaded onto the silica particles and optical spectroscopy was used to probe for the maximum loading by analyzing whether QDs remain in the supernatant of the QD loaded silica particles after centrifugation. The absorbance spectra of the used QDs in water are shown in **Fig. S4a** for two different concentrations. Different volumes of 23.6 μM aqueous quantum dot solutions were added to 1 mL aqueous silica particles (10 mg/mL) coated with PDADMAC following route (ii). The solutions were then mixed and centrifuged and the absorbance spectra of their supernatants are shown in **Fig. S4b**. When the QD concentration of the mixture was 2.36 μM, the supernatant was strongly colored, so clearly not all QDs were loaded onto the silica particles. When the QD concentration was decreased, the QD optical signature in the supernatant faded and disappeared for a QD concentration of 0.83 μM, indicating that at this concentration all QDs were loaded onto the silica particles. The maximum loading efficiency of QD loading onto silica particles was calculated to be 6.3×10^{-2} nmol/mg.

The optical properties of the precursor materials, which were loaded onto the silica particles, and the respective doped silica particle product are shown in Fig. 3. The optical absorbance spectra of the respective dyes in aqueous solution (1 mg/mL concentration) show their typical optical signature (Fig. 3a). The corresponding dye doped silica particles prepared via route (*i*) were spectrally analyzed in their dry form using diffuse reflectance spectroscopy employing an integrating sphere. The optical signature is largely unchanged. Note that the inverted shape of

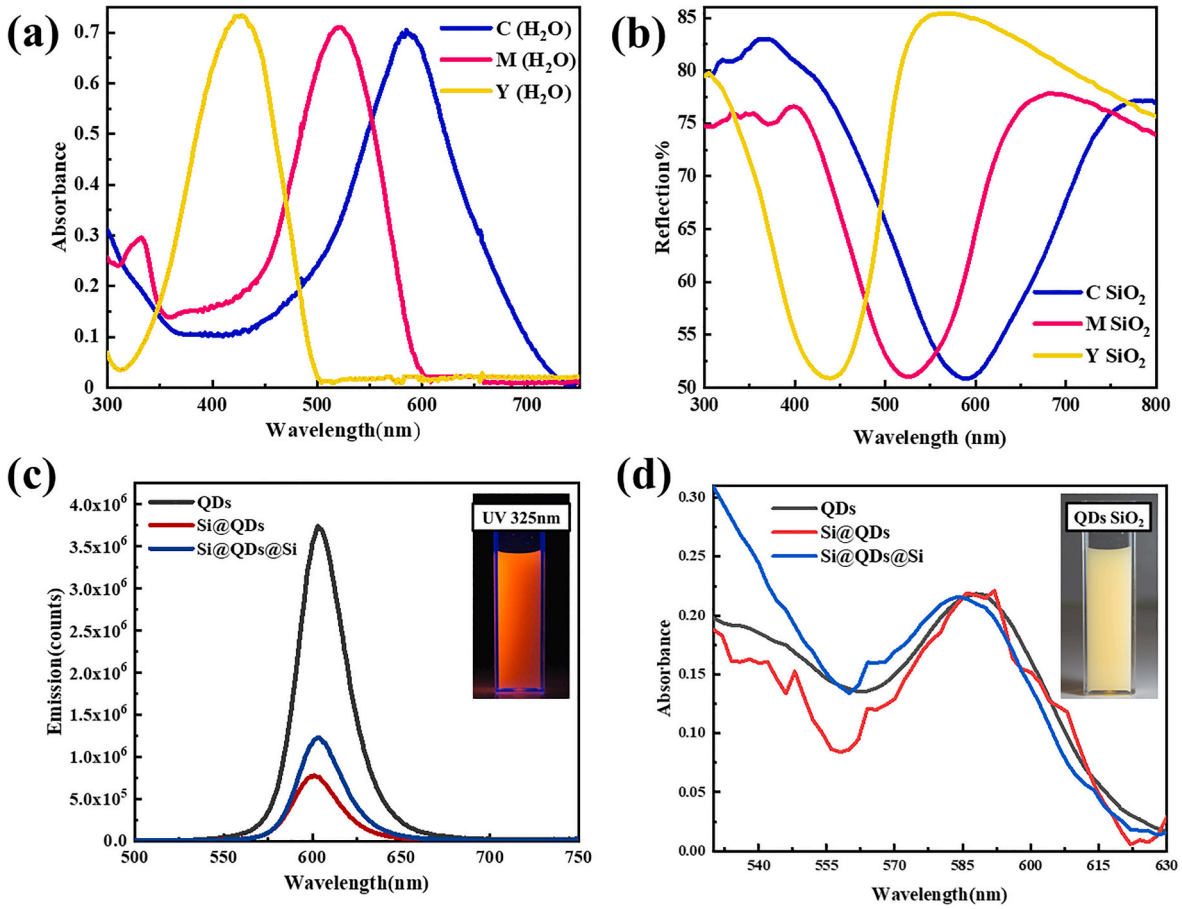

Fig. 3. Optical properties of the employed precursors and the loaded silica particles. (a) Absorbance spectra of the dyes in aqueous solution. (b) Diffuse reflectance spectra of the dye loaded SiO_2 particles. (c) Emission spectra of water soluble CdSe/ZnS QD in solution at pH 7, and the emission spectrum of the same QDs loaded onto SiO_2 particles and the same QDs loaded onto SiO_2 particles with and without silica shell termination. The spectra were collected using an excitation wavelength of 350 nm from different masses of material, which explains to difference in intensities. A photograph of water soluble CdSe/ZnS QD loaded SiO_2 particles exposed to UV light is shown in the inset. (d) The absorbance spectra of water soluble CdSe/ZnS QDs and the same QDs loaded onto SiO_2 particles with and without silica shell termination in solution at pH 7. The light scattering background was subtracted using a polynomial function and assuming Rayleigh scattering. The inset shows a photograph of the water soluble CdSe/ZnS QD loaded SiO_2 particles in ambient room lighting conditions.

the curve is due to the fact the powder spectrum is measured via its reflectance rather than absorption of light (Fig. 3b). The emission spectra of the CdSe/ZnS QD precursor and the CdSe/ZnS QD loaded silica particles in aqueous solution at pH 7 are shown in Fig. 3c, while the UV–Vis absorption spectrum is shown in Fig. 3d. The absorbance of the CdSe/ZnS QDs shows the typical profile of core-shell quantum dots, which is governed by the quantum confinement effect in semiconductor nanoparticles [27]. This results in discrete electronic energy levels that support the excitation of electron-hole pairs across the band gap by light, i.e. exciton generation. The decay of such excitons results in photoluminescence [28]. The emission spectrum of the QD loaded silica particles shows a distinct emission peak with the expected red-shift with respect to the QD absorption peak, which confirms the QD loading to the silica particles. Interestingly, the position of the emission peak (603 nm) is not shifted at the end of the loading step nor after the silica shelling process. Visually, the quantum dot loaded silica particles appear pale yellow with strong orange emission under ultra-violet light irradiation in the dark as shown in the insets to Fig. 3.

The morphology of the precursor nanoparticles and the silica particles loaded with dyes and quantum dots were investigated with electron microscopy, the results are shown in Fig. 4. Because the three CMY dye loaded silica particles employ the same synthesis method, only the yellow particles are shown here. SEM analysis shows that the dye-loaded and silica-shell-terminated, (Fig. 4a) yellow silica particles are very uniform and monodisperse. Fig. 4b shows an SEM image of negatively charged QD-loaded silica particles. Fig. 4c shows an SEM image of negatively charged QD-loaded silica particles with silica shell termination. A TEM image of the quantum dot loaded silica particles with silica shell termination is shown in Fig. 4d. The individual quantum dots are indicated by red circles, and a TEM image of quantum dots before loading are shown in the inset.

Additional electron microscopy images of all synthesis steps of the dye and QD loaded silica particles are shown in the *Supplementary Information*. **Fig. S5** summarizes the electron microscopy characterization of the individual synthesis steps for yellow dye doped silica particles using route(i). Uniform silica particles with smooth surface without impurities are shown at different magnifications in **Fig. S5 (a,b,c).** The corresponding S@P/D particles are shown in **Fig. S5 (d,e,f)** and appear to exhibit a thin shell coating due to the P/D coating. The silica terminated S@P/D@S particles are shown in **Fig. S5 (g,h,i)** and clearly show shell formation. The shells are accompanied by a slight increase in particle diameter, visible in the histograms of the size distribution in the insets to the corresponding SEM images. While the mean size of the silica particles is about 608 nm, the size of the S@P/D particles increases to about 616 nm, and the size of the corresponding S@P/D@S particles is about 625 nm after silica shell termination. **Fig. S6** summarizes the electron microscopy characterization of the individual synthesis steps for yellow dye doped silica particles using route (ii). The electron microscopy images of S@P, S@P@D and S@P@D@S particles are shown in **Fig. S6 (a,b,c), Fig. S6 (d,e,f)**, and **Fig. S6 (g,h,i)** respectively. Small non-uniformities on the particle surfaces are indicative of the coated layers. The size distributions of the particles in the different steps reveal that the mean size of S@P grew to about 616 nm from 608 nm for the bare particles. After yellow dye loading, the average size of the now S@P@D particles remained approximately unchanged as expected. After silica shell termination, the S@P@D@S particles reached a final diameter of about 628 nm. Comparing the final diameters of S@P@D@S (628 nm) and the S@P/D@S (625 nm) particles, we can conclude that the size increase is approximately the same for both synthesis routes, i.e. routes (i) and (ii). Route(ii) was also employed for the loading with QDs and the corresponding electron microscopy images of the S@P@Q and S@P@Q@S particles are shown in **Fig. S7 (a,b,c)** and **Fig. S7 (d,e,f)** respectively. In this case, the mean diameter increased by approximately 15 nm during silica shell termination.

The silica shell termination for these particles fulfills two important requirements. On the one hand, a universal silica shell termination enables a uniform particle surface chemistry to be created despite the diverse chemistry of the different doping agents. Secondly, the silica shell prevents dye leaching, which can be detrimental in biomedical applications [29] or in electronic applications such as displays [30].

We studied the leakage of both the dye and QD doped silica particles with silica shell termination over an extended time. The results are shown in **Fig. S8 a** for the dye doped particles, and in **Fig. S8 b** for the QD doped particles, where we measured the absorbance of the supernatant after centrifugation of the particle suspensions. After the absorbance measurement, the supernatant and the precipitated particles were redispersed. This was repeated for 7 days and no increase in intensity was observed. The inset in **Fig. S8a** shows a photograph of the centrifuged suspensions with the colored precipitates and clear supernatant.

The silica shell termination also preserves the fluorescence properties of the QD doped silica particles. As shown in Fig. 5, at pH 7 the emission maximum of QDs blue-shifted slightly from 603 nm to 601 nm when the particles were loaded on the silica. However, when the silica shell was added, the maximum returned to be at 603 nm. A blue shift in

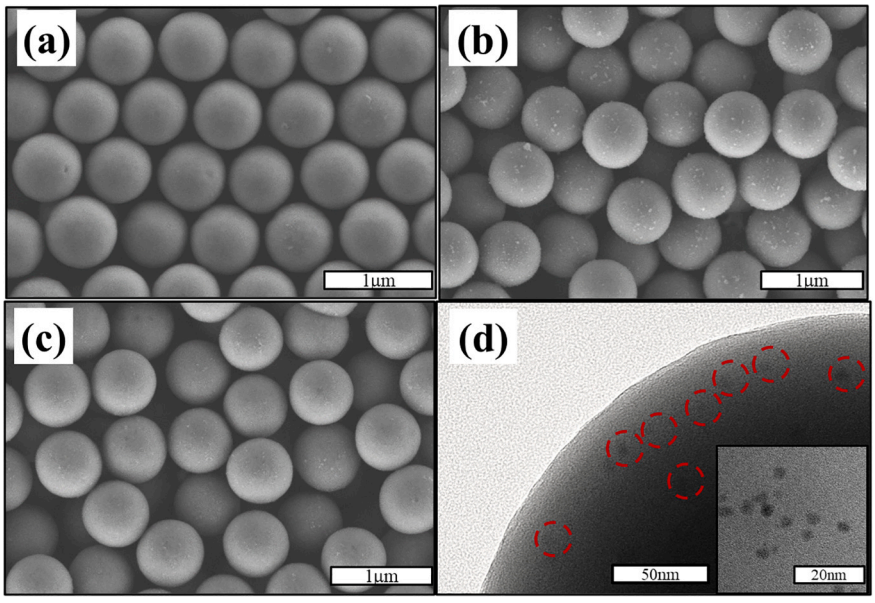

Fig. 4. Electron microscopy images of dye and quantum dot loaded silica particles. (a) Yellow dye loaded silica particles terminated with a silica shell. (b) QDs coated on the silica particles. (c) QDs coated on the silica particles terminated with a silica shell. (d) TEM image of a quantum dot loaded silica particle with silica shell termination. The individual quantum dots are indicated by red circles and a TEM image of quantum dots before loading are shown in the inset. (For interpretation of the references to colour in this figure legend, the reader is referred to the web version of this article.)

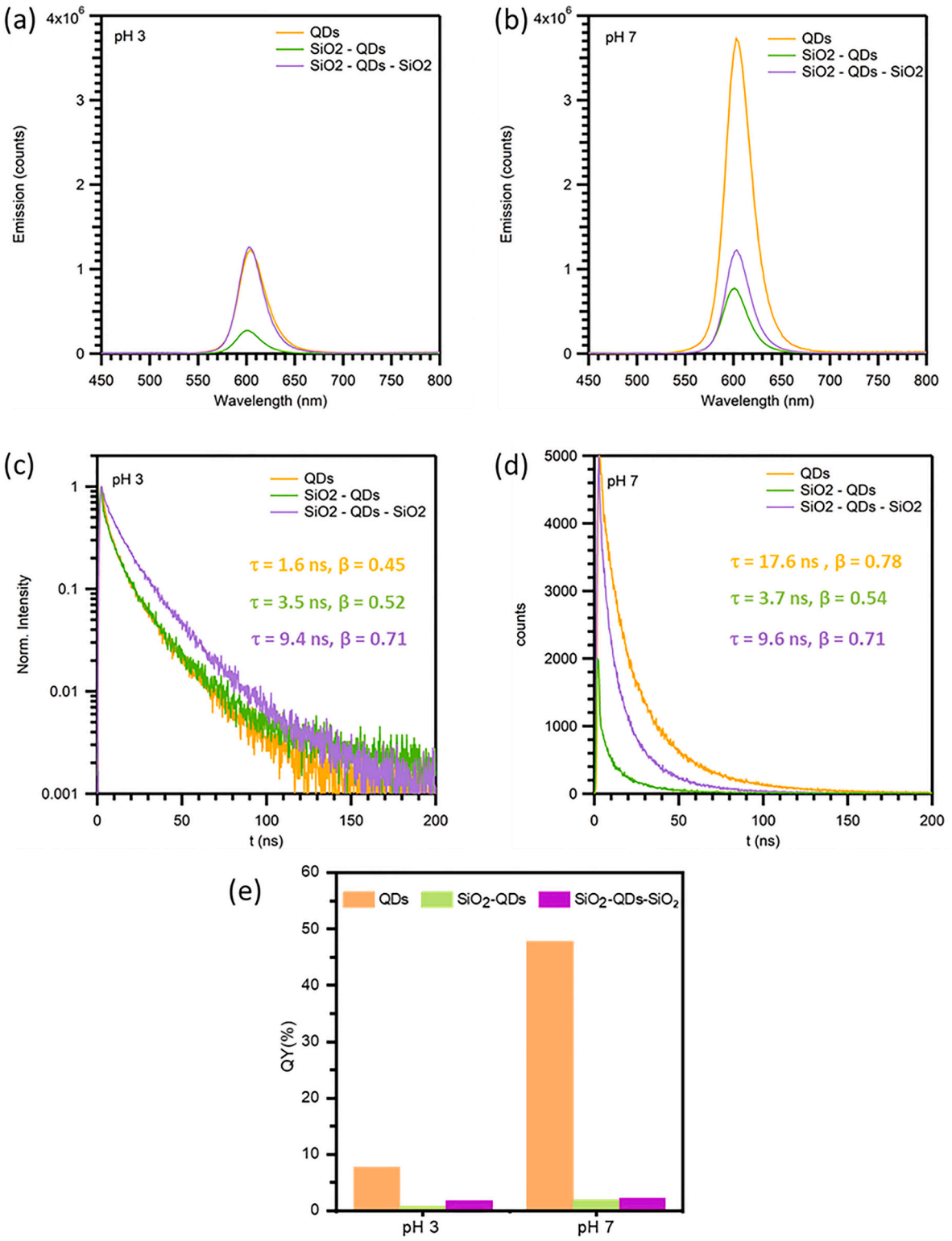

Fig. 5. Optical characterization of CdSe/ZnS QDs (QDs, yellow trace), QDs loaded on silica (SiO_2-QDs, green trace) and QDs-loaded silica particles with a silica shell (SiO_2-QDs- SiO_2, purple trace) in water. (a) Steady state fluorescence spectra at pH 3. (b) Steady state fluorescence spectra at pH 7. (c) Fluorescence decay curves at pH 3, with the results of the stretched exponential fit. (d) Fluorescence decay curves at pH 7, with the results of the stretched exponential fit. (e) Fluorescence quantum yield (QY) at pH 3 and 7. The mass of material used to collect the spectra was the same between pH 3 and pH 7, but the mass of material differed between spectra collected for QDs versus SiO_2-QDs and SiO_2-QDs-SiO_2 particles. (For interpretation of the references to colour in this figure legend, the reader is referred to the web version of this article.)

QDs is usually interpreted as dissolution of the nanocrystals [31], but this seems not to be the case in this system since the emission peak returned to its original value after the silica shelling. This relative insensitivity of the QDs emission to the local environment is likely due to the ZnS shells, which are known to physically and electronically insulate the CdSe core from its environment [32]. At pH 3 a similar trend was observed (Fig. 5a), with the emission maximum blue shifting from 603 nm to 601 nm after silica loading, and then red shifting to 604 nm after silica shelling. Fluorescence lifetime measurements in Fig. 5c-d were fitted with a stretched exponential function $A\ exp(-t/\tau)^{\beta}$, normally used to describe the luminescence decay in QDs, where τ is the fluorescence lifetime and β is the stretching factor. β accounts for recombination pathways provided by defects inside the nanocrystal or by traps at the nanocrystal surface [33]. At pH 7, τ decreased from 17.6 ns for QDs in solution ($\beta = 0.78$) to 3.7 ns for QDs loaded on silica ($\beta = 0.54$), and then increased to 9.6 ns after the silica shell was added ($\beta = 0.71$). This trend mirrored the quantum yield (QY) measurements of Fig. 5e, where the QY dropped from 47.8% to 1.9% after silica loading, partially recovering to 2.2% after silica shelling. These results suggest that the QD fluorescence is probably quenched during the loading process. At pH 3 the values of fluorescence intensity, QY and lifetime of QDs in solution were lower than at pH 7. This is a well-known phenomenon for QDs prepared via PSMA encapsulation, which start to aggregate below pH 4 [25]. Interestingly, the decay curves at pH 3 for QDs loaded on silica ($\tau = 3.5$, $\beta = 0.52$) and with the silica shell ($\tau = 9.4$, $\beta = 0.71$) are similar to the curves at pH 7. While the QY of QDs loaded on silica is lower at pH 3 (0.82%) than at pH 7 (1.9%), the QY after silica shelling in pH 3 (1.85%) is comparable to the value at pH 7 (2.2%). It has been reported that the use of silica in conjunction with polymers might help to stabilize QDs at acidic pH [34].

4. Conclusion

We have demonstrated a new strategy for synthesizing doped silica nanoparticles with a core-shell structure and demonstrated the universality of the method by employing it to encapsulate a variety of dyes as well as quantum dots into the silica particles. Electrostatic adsorption of negatively charged dyes onto negatively charged silica spheres was achieved using PDADMAC as a bridge and the particles were terminated with a benign silica shell. Thus, strongly colored and photoluminescent silica particles were obtained. The quantum dot loaded silica particles showed reasonable emission even at acidic pH values due to the SiO_2 protective shell. Electron microscopy investigation revealed that the PDADMAC based shell is about 4 nm thick, while the outer silica shell features a thickness of 5–6 nm. Stability measurements confirmed that these particles were essentially leakage free over a timeframe of 7 days. Furthermore, the optical properties of the doped and silica terminated particles are shown to inherit the optical properties of the dopants. The presented method is simple, environmentally friendly, inexpensive and there are no obstacles to large-scale production. We envisage application of these particles as labels in biomedicine and as ink for electronic devices such as reflective displays.

Declaration of Competing Interest

The authors declare that they have no known competing financial interests or personal relationships that could have appeared to influence the work reported in this paper.

Acknowledgements

This work has been funded by the Guangdong Innovative and Entrepreneurial Team Program (No. 2016ZT06C517), the Science and Technology Program of Guangdong (No. 2021A0505030014), Guangdong Basic and Applied Basic Research Foundation (No. 2019B1515120037 and No. 2019A1515011631), and the Australian Government through Australian Research Council Grant CE170100026. E.M.A. acknowledges a Feodor Lynen Research Fellowship by the Alexander von Humboldt Foundation. FL acknowledges the Japan Society for the Promotion of Science for the International Research Fellowship.

Appendix A. Supplementary data

Supplementary data to this article can be found online at https://doi.org/10.1016/j.colcom.2022.100594.

References

[1] S. Li, F. Wang, X.W. He, W.Y. Li, Y.K. Zhang, One-pot hydrothermal preparation of gadolinium-doped silicon nanoparticles as a dual-modal probe for multicolor fluorescence and magnetic resonance imaging, J. Mater. Chem. B 6 (2018) 3358–3365, https://doi.org/10.1039/c8tb00415c.
[2] M. Qhobosheane, S. Santra, P. Zhang, W. Tan, Biochemically functionalized silica nanoparticles, Analyst. 126 (2001) 1274–1278, https://doi.org/10.1039/b101489g.
[3] L. Latterini, M. Amelia, Sensing proteins with luminescent silica nanoparticles, Langmuir. 25 (2009) 4767–4773, https://doi.org/10.1021/la803934f.
[4] X. Meng, L. Qiang, J. Wei, H. Shi, Preparation of electrophoretic nanoparticles for electronic paper, J. Nanosci. Nanotechnol. 14 (2014) 1617–1630, https://doi.org/10.1166/jnn.2014.9136.
[5] L. Wang, K. Wang, S. Santra, X. Zhao, L.R. Hilliard, J.E. Smith, Y. Wu, W. Tan, Watching silica nanoparticles glow in the biological world, Anal. Chem. 78 (2006) 646–654, https://doi.org/10.1021/ac0693619.
[6] A. van Blaaderen, A. Vrij, Synthesis and characterization of colloidal dispersions of fluorescent, monodisperse silica spheres, Langmuir. 8 (1992) 2921–2931.
[7] D. Zhang, Z. Wu, J. Xu, J. Liang, J. Li, W. Yang, Tuning the emission properties of Ru(phen)32+ doped silica nanoparticles by changing the addition time of the dye during the stöber process, Langmuir. 26 (2010) 6657–6662, https://doi.org/10.1021/la903995r.
[8] X. Zhao, R.P. Bagwe, W. Tan, Development of organic-dye-doped silica nanoparticles in a reverse microemulsion, Adv. Mater. 16 (2004) 173–176, https://doi.org/10.1002/adma.200305622.
[9] J. Godoy-Navajas, M.P. Aguilar-Caballos, A. Gómez-Hens, Synthesis and characterization of oxazine-doped silica nanoparticles for their potential use as stable fluorescent reagents, J. Fluoresc. 20 (2010) 171–180, https://doi.org/10.1007/s10895-009-0535-2.
[10] A. Imhof, M. Megens, J.J. Engelberts, D.T.N. De Lang, R. Sprik, W.L. Vos, Spectroscopy of fluorescein (FITC) dyed colloidal silica spheres, J. Phys. Chem. B 103 (1999) 1408–1415, https://doi.org/10.1021/jp983241q.
[11] J. Liang, Z. Xue, J. Xu, J. Li, H. Zhang, W. Yang, Highly efficient incorporation of amino-reactive dyes into silica particles by a multi-step approach, Coll. Surf. A Physicochem. Eng. Asp. 426 (2013) 33–38, https://doi.org/10.1016/j.colsurfa.2013.02.064.
[12] W. Stöber, A. Fink, E. Bohn, Controlled growth of monodisperse silica spheres in the micron size range, J. Colloid Interface Sci. 26 (1968) 62–69.
[13] L. Jiao, J.R. Regalbuto, The synthesis of highly dispersed noble and base metals on silica via strong electrostatic adsorption: I. amorphous silica, J. Catal. 260 (2008) 329–341, https://doi.org/10.1016/j.jcat.2008.09.022.
[14] L.M. Rossi, L. Shi, F.H. Quina, Z. Rosenzweig, Stöber Synthesis of Monodispersed Luminescent Silica Nanoparticles for Bioanalytical Assays 21, 2005, pp. 4277–4280, https://doi.org/10.1021/la0504098.
[15] T. Kornprobst, J. Plank, Photodegradation of rhodamine B in presence of CaO and NiO-CaO catalysts, Int. J. Photoenergy. 2012 (2012) 1–7, https://doi.org/10.1155/2012/398230.
[16] V. Gubala, G. Giovannini, F. Kunc, M.P. Monopoli, C.J. Moore, Dye-doped silica nanoparticles: synthesis, surface chemistry and bioapplications, Cancer Nanotechnol. (2020), https://doi.org/10.1186/s12645-019-0056-x.
[17] T. Nann, P. Mulvaney, Single quantum dots in spherical silica particles, Angew. Chem. Int. Ed. 43 (2004) 5393–5396, https://doi.org/10.1002/anie.200460752.
[18] C. Wang, Q. Ma, W. Dou, S. Kanwal, G. Wang, P. Yuan, X. Su, Synthesis of aqueous CdTe quantum dots embedded silica nanoparticles and their applications as fluorescence probes, Talanta. 77 (2009) 1358–1364, https://doi.org/10.1016/j.talanta.2008.09.018.
[19] H.M. Kim, C. Oh, J. An, S. Baek, S. Bock, J. Kim, H.S. Jung, H. Song, J.W. Kim, A. Jo, D.E. Kim, W.Y. Rho, J.Y. Jang, G.J. Cheon, H.J. Im, B.H. Jun, Multi-quantum dots-embedded silica-encapsulated nanoparticle-based lateral flow assay for highly sensitive exosome detection, Nanomaterials. 11 (2021) 1–10, https://doi.org/10.3390/nano11030768.
[20] Y. Ha, H.S. Jung, S. Jeong, H.M. Kim, T.H. Kim, M.G. Cha, E.J. Kang, X.H. Pham, D. H. Jeong, B.H. Jun, Fabrication of remarkably bright QD densely-embedded silica nanoparticle, Bull. Kor. Chem. Soc. 40 (2019) 9–13, https://doi.org/10.1002/bkcs.11629.
[21] B.H. Jun, D.W. Hwang, H.S. Jung, J. Jang, H. Kim, H. Kang, T. Kang, S. Kyeong, H. Lee, D.H. Jeong, K.W. Kang, H. Youn, D.S. Lee, Y.S. Lee, Ultrasensitive, biocompatible, quantum-dot-embedded silica nanoparticles for bioimaging, Adv. Funct. Mater. 22 (2012) 1843–1849, https://doi.org/10.1002/adfm.201102930.

[22] H. Yoo, H.S. Jang, K. Lee, K. Woo, Quantum dot-layer-encapsulated and phenyl-functionalized silica spheres for highly luminous, colour rendering, and stable white light-emitting diodes, Nanoscale. 7 (2015) 12860–12867, https://doi.org/10.1039/c5nr02991k.
[23] C. Graf, S. Dembski, A. Hofmann, E. Rühl, A general method for the controlled embedding of nanoparticles in silica colloids, Langmuir. 22 (2006) 5604–5610, https://doi.org/10.1021/la060136w.
[24] H. Yang, E.M. Akinoglu, L. Guo, M. Jin, G. Zhou, M. Giersig, L. Shui, P. Mulvaney, A PTFE helical capillary microreactor for the high throughput synthesis of monodisperse silica particles, Chem. Eng. J. 401 (2020), 126063, https://doi.org/10.1016/j.cej.2020.126063.
[25] E.E. Lees, T.L. Nguyen, A.H.A. Clayton, P. Mulvaney, The preparation of colloidally stable, water-soluble, biocompatible, semiconductor nanocrystals with a small hydrodynamic diameter, ACS Nano 3 (2009) 1121–1128, https://doi.org/10.1021/nn900144n.
[26] J.J. Li, Y.A. Wang, W. Guo, J.C. Keay, T.D. Mishima, M.B. Johnson, X. Peng, Large-scale synthesis of nearly monodisperse CdSe/CdS core/shell nanocrystals using air-stable reagents via successive ion layer adsorption and reaction, J. Am. Chem. Soc. 125 (2003) 12567–12575, https://doi.org/10.1021/ja0363563.
[27] G. Pathak, G. Hegde, V. Prasad, Octadecylamine-capped CdSe/ZnS quantum dot dispersed cholesteric liquid crystal for potential display application: investigation on photoluminescence and UV absorbance, Liq. Cryst. 48 (2021) 579–587, https://doi.org/10.1080/02678292.2020.1799085.
[28] L. Wang, W. Tan, Multicolor FRET silica nanoparticles by single wavelength excitation, Nano Lett. 6 (2006) 84–88, https://doi.org/10.1021/nl052105b.
[29] A.M. Wagner, J.M. Knipe, G. Orive, N.A. Peppas, Quantum dots in biomedical applications, Acta Biomater. 94 (2019) 44–63, https://doi.org/10.1016/j.actbio.2019.05.022.
[30] P. Yin, G. Wu, W. Qin, X. Chen, M. Wang, H. Chen, CYM and RGB colored electronic inks based on silica-coated organic pigments for full-color electrophoretic displays, J. Mater. Chem. C 1 (2013) 843–849, https://doi.org/10.1039/c2tc00344a.
[31] C. Bullen, P. Mulvaney, The effects of chemisorption on the luminescence of CdSe quantum dots, Langmuir. 22 (2006) 3007–3013, https://doi.org/10.1021/la051898e.
[32] J. Van Embden, J. Jasieniak, D.E. Gómez, P. Mulvaney, M. Giersig, Review of the synthetic chemistry involved in the production of core/shell semiconductor nanocrystals, Aust. J. Chem. 60 (2007) 457–471, https://doi.org/10.1071/CH07046.
[33] J. Van Embden, J. Jasieniak, P. Mulvaney, Mapping the optical properties of CdSe/CdS heterostructure nanocrystals: the effects of core size and shell thickness, J. Am. Chem. Soc. 131 (2009) 14299–14309, https://doi.org/10.1021/ja9030209.
[34] X. Hu, X. Gao, Silica-polymer dual layer-encapsulated quantum dots with remarkable stability, ACS Nano 4 (2010) 6080–6086, https://doi.org/10.1021/nn1017044.